Biomaterials 33 (2012) 614–623

Contents lists available at SciVerse ScienceDirect

Biomaterials

journal homepage: www.elsevier.com/locate/biomaterials

Bioreducible poly(amidoamine)s as carriers for intracellular protein delivery to intestinal cells

Shmuel Cohen [a,1], Grégory Coué [b,1], Delila Beno [a], Rafi Korenstein [a], Johan F.J. Engbersen [b,*]

[a] Department of Physiology and Pharmacology, Sackler Faculty of Medicine, Tel Aviv University, Tel-Aviv, Israel
[b] Department of Biomedical Chemistry, MIRA Institute for Biomedical Technology & Technical Medicine, Faculty of Science and Technology, University of Twente, Enschede, The Netherlands

ARTICLE INFO

Article history:
Received 7 September 2011
Accepted 25 September 2011
Available online 19 October 2011

Keywords:
Poly(amidoamine)
Intracellular protein delivery
Mucoadhesive nanoparticles
Bioresponsive nanoparticles
Bioreducible polymer
Endosomal uptake

ABSTRACT

An effective intracellular protein delivery system was developed based on linear poly(amidoamine)s (PAAs) that form self-assembled cationic nanocomplexes with oppositely charged proteins. Two differently functionalized PAAs were synthesized by Michael-type polyaddition of 4-amino-1-butanol (ABOL) to cystamine bisacrylamide (CBA) and to bisacryloylpiperazine (BAP), yielding p(CBA-ABOL) and p(BAP-ABOL), respectively. These water-soluble PAAs efficiently condense human serum albumin (HSA) by self-assembly into stable nanoscaled and positively-charged complexes. The disulfide-containing p(CBA-ABOL)/HSA nanocomplexes exhibited high mucoadhesive properties and, while stable under neutral (extracellular) conditions, rapidly destabilized in a reductive (intracellular) environment due to the cleavage of the repetitive disulfide linkages in the CBA units of the polymer. Human-derived intestinal Caco-2/TC7 cells and HT29-MTX mucus secreting cells were exposed to these PAAs/HSA nanoparticles and the extent of their uptake and the localization within endosomal compartments were examined. The higher uptake of p(CBA-ABOL)/HSA than that of p(BAP-ABOL)/HSA suggests that the mucoadhesive properties of the p(CBA-ABOL) are beneficial to the uptake process. The transported HSA was located within early endosomes, lysosomes and the cytosol. The enhanced uptake of the p(CBA-ABOL)/HSA nanoparticles, observed in the presence of Cyclosporin A, a non-specific Multi Drug Resistance (MDR) blocker, indicates the possible efflux of these nanoparticles through MDR transporters. The results show that bioreducible PAAs have excellent properties for intracellular protein delivery, and should be applicative in oral protein delivery.

1. Introduction

Peroral drug application is considered as the most convenient and preferred route for therapeutic protein administration, especially in long-term treatment. However, this route is associated with a great number of hurdles that have to be overcome before the drug can exert its therapeutic activity. The bioavailability of therapeutic proteins via the oral administration route is very low due to (i) physical and chemical instability and fast enzymatic degradation in the gastrointestinal tract [1,2], (ii) charge repulsion of proteins from negatively-charged cell membranes and mucosa cells, and (iii) slow and ineffective transport of large size and hydrophilic proteins through compartmental cellular barriers [3,4]. Encapsulation of proteins in polymeric nanocarriers that protect the proteins during transport to their intracellular destination is a possible strategy to overcome these hurdles. A promising approach to achieve improved stability and enhanced uptake compared to the free peptides and proteins is the use of appropriate biodegradable synthetic polymers that form self-assembled nanocomplexes with the peptide or protein drugs of interest.

For efficient delivery via the intestine, the mucoadhesion of the colloidal carriers has been reported to be one of the most important properties to improve the bioavailability of poorly absorptive drugs [3–7]. Mucoadhesive carriers which adhere to the mucus layer of intestinal mucosal membranes are expected to prolong the residence time at the local site of absorption, leading to increased drug absorption through the intestinal cell layer. An interesting possibility to increase the mucoadhesive properties of a polymeric carrier is the introduction of disulfide bonds in the polymer backbone since the repetitive disulfide linkages in the polymer can react with thiol groups and disulfide groups in the mucus [8–12].

* Corresponding author. Tel.: +31 53 489 2926; fax: +31 53 489 2155.
E-mail address: J.F.J.Engbersen@utwente.nl (J.F.J. Engbersen).
[1] Contributed equally.

0142-9612/$ – see front matter © 2011 Elsevier Ltd. All rights reserved.
doi:10.1016/j.biomaterials.2011.09.085

In this study we have evaluated two differently functionalized poly(amidoamine)s (PAAs), one PAA comprising repetitive disulfide linkages (SS-PAA), and one lacking disulfide linkages in their polymer backbone, for their efficacy to deliver the model protein human serum albumin (HSA) to human intestinal epithelial Caco-2/TC7 cells, and co-cultures Caco-2/TC7 and HT29-MTX mucus secreting cells. These cells are widely used in pharmaceutical research as a model for the human small intestinal mucosa to predict the uptake of orally administered drugs via the intestinal route. The PAAs have been chosen as carriers since these polymers can be synthesized with a great variety in structure by polyaddition of primary and secondary amines to bisacrylamides. These cationic polymers are water-soluble, biodegradable and have lower cytotoxicity than other usual polycationic vectors [13–16]. PAAs have shown high potential in biomedical applications [17,18], particularly for use as intracytoplasmic and endosomolytic vectors for the delivery of anticancer drugs [19,20], proteins [21–23] and nucleotides [24–28]. The tertiary amines in the main chain of the PAAs give these polymers high buffer capacity in the pH range 5.1–7.4 and this property facilitates PAA nanocomplexes once taken up by cells to escape from the endosomes by increasing polymer-membrane interaction and the proton sponge effect [13,29,30]. Consequently, degradation of the therapeutic cargo by lysosomal enzymes is prevented [31].

To evaluate the effect of the presence of repetitive disulfide groups in the main chain of SS-PAAs on the mucoadhesive criteria, we have synthesized the disulfide-containing polymer p(CBA-ABOL) and the reference polymer p(BAP-ABOL), lacking disulfide linkages, by Michael-type polyaddition of 4-amino-1-butanol (ABOL) to cystamine bisacrylamide (CBA) and to bisacryloylpiperazine (BAP), respectively. In addition, the p(CBA-ABOL) polymer is relatively stable in the extracellular medium but is prone to fast degradation in the intracellular environment due to reductive cleavage of the disulfide linkages, thereby releasing its therapeutic payload and diminishing potential cytotoxicity effects of the polymer [32–34]. By simply mixing negatively-charged HSA (pI = 5.3) and positively-charged PAA at neutral pH, self-assembled polyelectrolyte complexes (PECs) with nanosized dimensions are formed, as is schematically represented in Scheme 1. The PECs possess cationic surface charge, which makes them amenable to bind to negatively-charged cell membranes and internalize into the cells [35].

2. Materials and methods

2.1. Materials

Human serum albumin–fluorescein isothiocyanate conjugate (FITC-HSA, ~10 mol FITC per mol HSA) was obtained from Sigma. All monomers, 4-amino-1-butanol (ABOL, Aldrich), Mono-Boc-protected diaminobutane (MBDAB, Fluka), *N,N′*-cystamine bisacrylamide (CBA, Polysciences, USA), 1,4-bis(acryloyl)piperazine (BAP, Sigma–Aldrich) were purchased in the highest purity and used without further purification. HEPES (Sigma), dithiothreitol (DTT, Sigma–Aldrich), trifluoroacetic acid (TFA, Aldrich), porcine gastric mucus (Sigma), anhydrous dimethylsulfoxide (DMSO, Acros Organics), and methanol (MeOH, Biosolve) were used as received. The amine-reactive Alexa Fluor® 633 carboxylic acid, succinimidyl ester (AF633) was purchased from Invitrogen. Deionized water (DI water) was obtained from a MilliQ water purification system (Millipore, France).

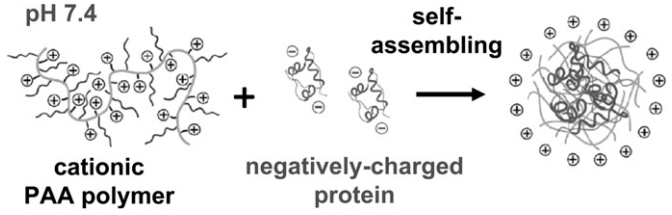

Scheme 1. Self-assembling formation of nanocomplexes at neutral pH by charge attraction between a negatively-charged protein (such as human serum albumin) and a positively-charged polymer (PAA).

2.2. Synthesis of poly(amidoamine)s (PAAs)

The SS-PAA polymer, p(CBA-ABOL), was synthesized by Michael polyaddition of the primary amine monomer ABOL to CBA in equimolar monomeric ratios in MeOH/water 4/1, as described previously [27]. The PAA polymer analog lacking the disulfide moieties, p(BAP-ABOL), was synthesized similarly using BAP and ABOL as the monomers. In this case only DI water was used as the solvent [27]. The resulting polymers, collected in their HCl-salt form as white solid powder after freeze-drying, have a good solubility in water. For both polymers the yield was *ca.* 45% after ultrafiltration and lyophilization.

2.3. Synthesis of fluorescently labeled PAAs

The far-red fluorophore AF633 (λ_{em} = 647 nm) was chosen for labeling of the PAA polymers since the most common fluorescent label for detection in the red channel, Rhodamine B, is not usable as its fluorescence emission (λ_{em} = 610 nm) partly overlaps with the emission of fluorescein-HSA (λ_{em} = 525 nm) in the green channel. The AF633-labeled PAAs were prepared from copolymers having 10 mol% of the hydroxybutyl groups in the side chain substituted by aminobutyl groups. To synthesize these polymers, copolymers of (CBA-ABOL) and p(BAP-ABOL) were prepared by Michael addition of bisacrylamide (CBA or BAP, respectively) to a 9/1 mixture of amines, ABOL and MBDAB, followed by Boc-deprotection of the MBDAB units. Typically, p(CBA-ABOL/MBDAB) copolymer was synthesized by adding CBA (2.63 g, 10.75 mmol), ABOL (0.88 g, 9.67 mmol) and MBDAB (0.21 g, 1.08 mmol) into a brown reaction flask with 5 ml of a 4/1 (v/v) MeOH/DI water mixture as a solvent. The reaction mixture was allowed to proceed for 10 days at 45 °C in the dark under nitrogen atmosphere, yielding to a viscous solution. Subsequently, 10 mol% excess of ABOL (0.09 g, 0.11 mmol) was added to consume any unreacted acrylamide groups and stirring was continued for two days at 45 °C. The p(CBA-ABOL/MBDAB) polymer, containing Boc-protected amine in the side chain, was obtained in *ca.* 45% yield after isolation by exhaustive ultrafiltration (3 kg/mol cut-off) with acidified DI water (pH ~5), followed by freeze-drying. Deprotection of Boc-protected amino groups of the side chain of the polymer was performed in a mixture of TFA/MeOH overnight, yielding to the copolymers p(CBA-ABOL/DAB) with a 9/1 ratio of hydroxyl and primary amino groups in the side chains. Next, the reaction solution was diluted with DI water and adjusted to pH ~5 using a 1M NaOH solution and the resulting polymer solution was purified by ultrafiltration (3 kg/mol cut-off) with acidified DI water (pH ~5). The p(CBA-ABOL/DAB) polymer was recovered in its HCl-salt form as a white solid after lyophilization. The complete removal of the Boc protective groups was confirmed by the disappearance of the *tert*-butyl signal at 1.5 ppm in the ^{1}H NMR spectra after addition of TFA to the copolymer, yielding to the polymer with the free primary amine groups in the side chains. The primary amines were reacted with the amine-reactive AF633 carboxylic acid, succinimidyl ester, for fluorescent labeling of the polymer. In a typical example, for the synthesis of fluorescently-labeled AF633-p(CBA-ABOL), AF633 (2.5 mg, 2.08 μmol) in anhydrous DMSO was mixed with the p(CBA-ABOL/DAB) copolymer (146 mg, 41.60 μmol free NH_2) in 2 ml of sodium bicarbonate buffer (0.1 M, pH 8.3) and the solution was stirred overnight at room temperature. Then, the resultant solution was purified by ultrafiltration (1 kg/mol cut-off) with DI water. The labeled copolymer was isolated after freeze-drying. A similar experimental procedure was applied in the synthesis of AF633-p(BAP-ABOL).

2.4. Polymer characterization

The ^{1}H NMR spectra of the synthesized PAAs in D_2O were recorded on Varian Inova spectrometer operating at 300 MHz. The molecular weight and polydispersity (M_w/M_n) of the synthesized PAAs were determined by GPC relative to PEO standards (Polymer Labs) using a Viscotek GPCMax pump and autoinjector and two thermostated (30 °C) PL aquagel-OH 30 columns (8 μm, 300 × 7.5 mm, Polymer Labs, with a low-molar-mass separation range (200–40,000)). Data was collected using a TDA302 Tripledetector with RI, Visc and LS (7 and 90°). 0.3 M NaAc aqueous solution (pH 4.4) with 30% methanol was used as eluent at a flow rate of 0.7 ml/min.

2.5. Rheological studies

Rheological measurements were performed with a cone-plate (C35/28) rheometer (RotoVisco RT20, Haake GmbH, Karlsruhe, Germany). p(CBA-ABOL) and p(BAP-ABOL) were fully hydrated in 0.1 M phosphate buffer pH 6.8 to give a concentration of 6% (w/v). The polymer solutions were added to an equal volume of the 8% (w/v) solution of porcine gastric mucin. After an incubation period of 20 min at room temperature, the polymer–mucin incubates were transferred to the viscometer and allowed to equilibrate on the plate for 3 min at 25 °C. Dynamic oscillatory tests within the linear viscoelasticity region were performed at 1 Hz frequency. Frequency sweep measurements were also carried out with a frequency varying from 0.1 to 10 Hz. The storage modulus (G′) and the loss modulus (G″) of the disulfide-containing polymer p(CBA-ABOL) and the corresponding control polymer

p(BAP-ABOL) lacking the disulfide linkages (3% w/v), as well as mixtures of the same polymers with mucin (4% w/v) were determined. Rheological studies were performed with commercially-available mucin instead of native mucus giving more reproducible and comparable results. As references, polymer solutions were prepared in the same way but without adding mucin.

2.6. Characterization of PAA/HSA nanoparticles

2.6.1. Particle size and zeta-potential measurements

PAA/HSA nanocomplexes at different polymer/protein weight ratios ranging from 6/1 to 24/1 were prepared by adding a HEPES buffer solution (10 mM, pH 7.4) of PAA (800 μl) to a HEPES buffer solution (10 mM, pH 7.4) of HSA (200 μl, 600 μg/ml), followed by vortexing for 5 s and incubating at room temperature for 30 min. Particle size and surface charge measurements of the nanocomplexes were determined by dynamic light scattering (DLS) at 25 °C with a Zetasizer Nano ZS (Malvern Instruments, Malvern, UK) using a wavelength of 532 nm. The value was recorded as the mean of three measurements. The size distribution was given by the polydispersity index (PDI) in which a PDI of 1 indicates large variations in particle size and a PDI of 0 indicates no variation in particle size (i.e. an ideal monodispersed formulation).

2.6.2. Protein condensation and loading efficiency

To estimate the loading efficiency of the nanoparticles at neutral pH, solutions of PAA/HSA nanoparticles were prepared at polymer/protein weight ratios ranging from 6/1 to 24/1 according to the procedure described above. The nanoparticles were centrifuged at 14000 rpm for 30 min at 4 °C. Aliquots of supernatant were subsequently taken and their protein content determined by fluorescence spectroscopy (Safire2, Tecan, Canada) at an emission wavelength of 519 nm and an excitation wavelength of 495 nm. The actual loading efficiency was indirectly determined by measuring the difference between the total amount of HSA added to the solution and the amount of HSA in the free form in the supernatant. A calibration curve from solutions of various HSA concentrations was determined prior to this experiment. It was confirmed that free HSA were not precipitated from the solution by centrifugation.

2.6.3. Protein release from nanoparticles by disulfide reduction of the SS-PAAs

The release of protein from the nanoparticles at intracellular mimicking reductive conditions was measured using solutions of PAA/HSA nanoparticles prepared as described in Section 2.6.1 at polymer/protein weight ratio 24/1. The reducing agent DTT was added to a final concentration of 2.5 mM and the solution was incubated for 30 min. Subsequently, the solution was centrifuged at 14000 rpm for 30 min at 4 °C. Aliquots of supernatant were taken and their protein content was determined by measurement of the fluorescence intensity using a prior-determined calibration curve.

2.6.4. Protein release by acidification of the nanoparticles

The effect of pH decrease from 7.4 to 5.1 (mimicking endosomal pH decrease) on the particle size and surface charge of the nanoparticles was investigated at 25 °C by DLS measurements using a Zetasizer Nano ZS (Malvern Instruments, Malvern, UK) at a wavelength of 532 nm. The nanoparticle solution was titrated from pH 7.4 to pH 5.1 by regularly adding small aliquots of 0.25 M HCl solution using a MTP-2 multipurpose titrator (Malvern Instruments, Malvern, UK). Particle size and surface charge were determined every half-unit of pH. In another experiment, the release of protein from the nanoparticles upon acidification to pH 5, mimicking endosomal pH, was measured using solutions of PAA/HSA nanoparticles prepared at polymer/protein weight ratio 24/1 as previously. After acidification to pH 5 by addition of small amounts of 1 M HCl solution and incubation for 30 min, the nanoparticles were centrifuged at 14000 rpm for 30 min at 4 °C. Aliquots of supernatant were subsequently taken and their protein content was determined by fluorescence spectroscopy (λ_{em} = 519 nm, λ_{ex} = 495 nm) using a calibration curve. The percentage of released protein was calculated from the difference of the total amount of HSA originally present in the nanoparticle solution and the amount of HSA that is determined in the free form in the supernatant.

2.7. In vitro cellular uptake and cytotoxicity of the nanoparticles

2.7.1. Fluorescently labeled p(BAP-ABOL) and p(CBA-ABOL) nanoparticles with HSA

Polymer/protein nanoparticles made of p(CBA-ABOL) and p(BAP-ABOL) polymers and HSA were freshly prepared before every experiment at polymer/protein weight ratio 24/1 by adding 4 volume equivalents of p(CBA-ABOL) or p(BAP-ABOL) (3.60 mg/ml) to one equivalent of HSA (0.60 mg/ml), in 10 mM HEPES buffer. Before cell exposure, these nanoparticle solutions were diluted 1:10 in DMEM without fetal calf serum (FCS). Hence, the final polymer and protein concentrations for cell exposure experiments were 288 and 12 μg/ml, respectively. Before the FACS uptake studies, the fluorescence emission intensities of FITC-HSA and both nanoparticles made of the AF633-PAA polymers were measured at the excitation/emission wavelengths of for FITC (λ_{ex} = 490 nm, λ_{em} = 525 nm) and AF633 (λ_{ex} = 632 nm, λ_{em} = 647 nm). It was observed that the fluorescence intensities of HSA in the PAA nanoparticles were similar to those free in solution.

2.7.2. Cells and toxicity assays

All cells were used at passages 19–30, incubated at 37 °C in a humidified atmosphere of 95% air and 5% CO_2, and passaged at 80% confluence in a split ratio of 1/5 with a trypsin–ethylenediamine tetra acetic acid (EDTA) solution (0.25%). They were routinely grown in 75 cm^2 flasks in Dulbecco's modified Eagle's medium supplemented with 20% fetal bovine serum (FBS), 1% minimum essential medium (MEM) nonessential amino acids, 2 mM L-glutamine, 10 units/ml of penicillin, 10 μg/ml of streptomycin and 1.25 units/ml nystatin. Human intestinal epithelial Caco-2/TC7 cells which were used as a model for the intestine epithelial barrier were obtained from Dr. Monique Rousset, INSERM U505, Paris, France. HT29-MTX mucus secreting cells were obtained from Dr. Thécla Lesuffleur, Centre de Recherche Jean-Pierre Aubert – JPARC, INSERM U837, Lille, France. Toxicity level was determined using the AlamarBlue® test (AbD serotec) and the BCA protein assay (Pierce).

2.7.3. Flow cytometry analysis (FACS)

Uptake studies were conducted two days after cell plating. Caco-2/TC7 culture cells were grown to 70–80% confluence and were exposed to the PAA/HSA nanoparticles, PAA polymers alone and to free HSA in serum depleted culture medium for 2 h at 37 °C. The culture medium was then replaced by 10% FCS containing media with the same concentration of polymer/protein nanoparticles, and incubation was continued for additional 22 h at 37 °C. Non-specific blockers of permeability glycoprotein-multi drug resistance (P-gp-MDR) were also applied using exposure media containing 10 μM cyclosporin A (CsA). After exposure time, uptake was terminated by removal of the exposure medium and washing the cells twice with ice-cold PBS buffer. Trypsin–EDTA was used to suspend the adherent cells, followed by rinsing with DMEM supplemented with 10% FCS and suspending in final volume of 250 μl PBS buffer. As a control, the extent of adsorption of nanoparticles to the cell membrane surface was determined, by exposing cells to nanoparticles for 1 h at 4 °C. Thus, the reported uptake levels reflect the net results of uptake at 37 °C (total fluorescence obtained at 37 °C minus that measured at 4 °C).

2.7.4. Confocal microscopic imaging of nanoparticles uptake and localization

We used fluorescence confocal microscopy to detect internalization and the intracellular localization of the protein originating from the polymer/protein nanoparticles. Caco-2/TC7 cells were seeded onto 35-mm diameter glass bottomed dishes or cover slips at a density of 10^5 cells/cm^2 for 2–3 days. Cells were exposed to nanoparticles as described above in Section 2.7.3. Then, cells were rinsed twice in 10% FCS DMEM and further incubated for 30 min at 37 °C in 10% FCS medium supplemented with nuclear probe Hoechst 33342 (Invitrogen) and lysosomal staining probe LysoTracker Red DND-99 (Invitrogen) (λ_{ex} = 577 nm, λ_{em} = 590 nm), rinsed twice with PBS and subjected to confocal microscopy. Alternatively, cells were transiently transfected with Rab-5 (early endosome) and Cathepsin D (lysosome) coupled on N-terminal with monomeric Red Fluorescence Protein (RFP) (kindly gifted from Dr. Nancy J. Grant, Département de Neurotransmission et Sécrétion Neuroendocrine, Centre de Neurochimie, Strasbourg, France) and exposed to nanoparticles, then rinsed twice and scanned under a Zeiss 510 Meta inverted confocal microscope for estimation of uptake level and location of the nanoparticles. The photomultiplier tube (PMT) voltage was selected to produce images of approximately equal fluorescence intensity.

3. Results and discussion

3.1. Synthesis and characterization of PAAs

The SS-PAA polymer p(CBA-ABOL) with repetitive bioreducible disulfide linkages in its main chain was synthesized via Michael-type addition of the primary amine monomer ABOL to CBA. For comparison, p(BAP-ABOL), a PAA lacking disulfide linkages was prepared from polyaddition of ABOL to BAP. The polymers were coded in terms of the used monomers, as shown in Scheme 2. The resulting polymers, obtained in *ca.* 45% yield in their HCl-salt form as white powders after ultrafiltration and freeze-drying, have a good solubility in water. The ^{1}H NMR spectra of the synthesized PAAs were in full accordance with the expected structures. The absence of any proton signals between 5 and 7 ppm shows that the polymer did not contain any residual acrylamide end groups. The GPC measurements showed that the average molecular weights (M_w) of p(CBA-ABOL) and p(BAP-ABOL) were 5.9 and 5.5 kg/mol, respectively, (PDI = 1.13).

3.2. Mucoadhesive properties of the p(CBA-ABOL) polymer

The mucoadhesion of colloidal carriers represents one of the most important properties to improve the bioavailability of poorly

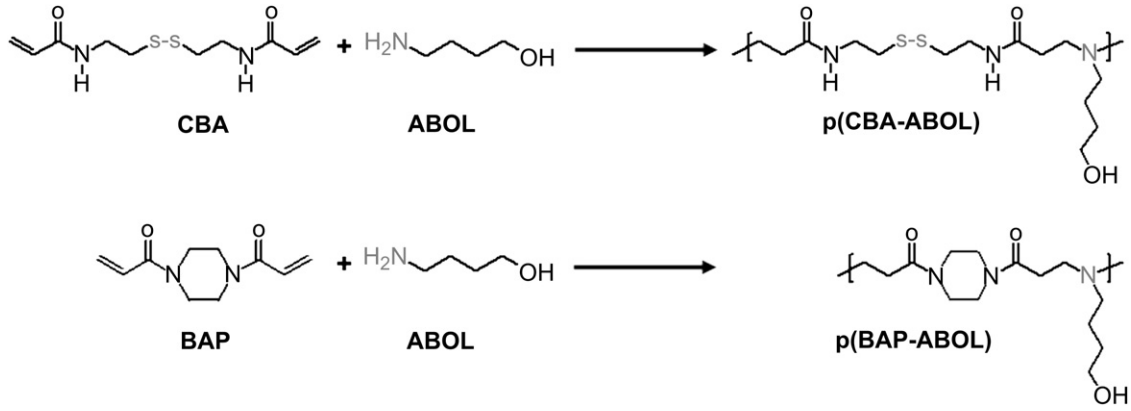

Scheme 2. Synthesis scheme of PAAs. The polymers were coded in terms of the bisacrylamide and primary amine monomers.

absorptive drugs such as proteins. Mucosal surfaces usually have distinct regions of mature mucins which are rich in cysteines, residues participating in establishing disulfide linkages within and among mucin monomers. We anticipated that the presence of disulfide linkages in p(CBA-ABOL) favorably contributes to the mucoadhesive properties of the polymer by disulfide exchange reactions with the thiol and disulfide groups in the mucus. To evaluate this concept, we have carried out rheology experiments of mucin mixed with solutions of the disulfide-containing p(CBA-ABOL) and p(BAP-ABOL), lacking disulfide bonds. Dynamic oscillatory measurements were performed within the linear viscoelasticity region by measuring the dynamic moduli (storage modulus G′ and the loss modulus G″) of the mixtures. This analysis provides information about the mechanical properties of the mixtures; increasing values of G′ and G″ indicating an increase of stiffness. The results are summarized in Fig. 1

A 4% (w/v) solution of mucin showed moderate viscosity with measured storage and loss moduli of 0.24 Pa and 0.14 Pa, respectively, whereas 3% polymer solutions of p(CBA-ABOL) and p(BAP-ABOL) in 0.1 M phosphate buffer did not show a significant increase in viscosity compared to pure buffer solution, with dynamic moduli close to zero. However, mixing mucin with p(CBA-ABOL) resulted in a 6.5–8 fold increase in storage and elastic moduli, with G′ and G″ of 1.57 Pa and 1.04 Pa, respectively. In contrast, mixing mucin with p(BAP-ABOL), the polymer lacking the disulfide linkages, only slightly increased rheological properties of the polymer/mucin mixture were observed. The different results between p(CBA-ABOL) and p(BAP-ABOL) suggest that the presence of the disulfide bonds in p(CBA-ABOL) is responsible for the higher viscosity obtained with this polymer. This increase in viscosity might be attributed to disulfide bond formation between the p(CBA-ABOL) polymer and mucin, due to exchange of disulfide linkages from the polymer with free thiol groups present in mucin. To obtain additional evidence for the formation of disulfide bonds between p(CBA-ABOL) and cysteine residues present in mucin, similar rheology measurements were performed in the presence of the disulfide bond reducing agent DTT. As shown in Fig. 1, addition of 2.5 mM DTT to the p(CBA-ABOL)/mucin mixture resulted in a dramatic decrease of the storage and loss moduli to values even lower than those determined for mucin only. For the p(BAP-ABOL)/mucin mixture, only a slight decrease of G′ and G″ is observed, which may also be explained by cleavage of mucus disulfide linkages.

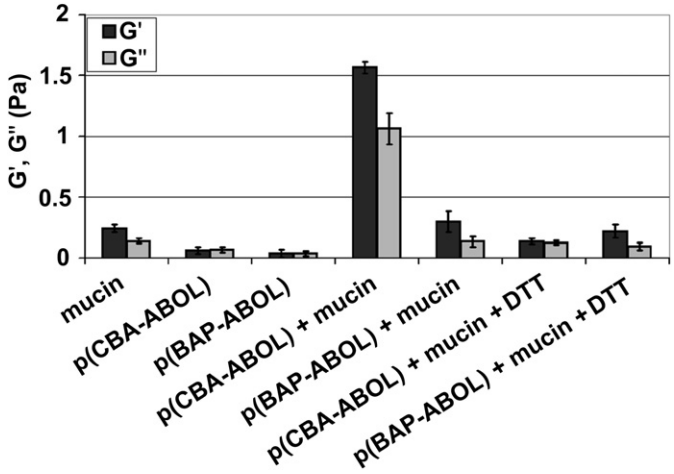

Fig. 1. Storage modulus G′ (black bars) and the loss modulus G″ (gray bars) of 3% (w/v) p(CBA-ABOL), p(BAP-ABOL) (control) and their mixtures with 4% (w/v) mucin in the presence or absence of DTT (free thiol). Oscillatory measurements were carried out at 1 Hz frequency at room temperature after an incubation period of 30 min. All indicated values are means of three experiments ± SD.

3.3. Protein loading of the PAA nanoparticles: physical characterization and loading efficiency

At physiological pH (pH 7.4), the PAAs are present as polycations due to partial protonation of the tertiary nitrogens in the polymer chain. Therefore, charge interaction with HSA can be expected since this protein, with an isoelectric point of 5.3, has a net negative charge under these conditions. DLS and zeta-potential measurements showed that both synthesized PAA polymers are capable to form nanosized polyelectrolyte complexes by self-assembly with HSA. The particles have sizes $\leq$ 200 nm with low polydispersity (PDI $<$ 0.15) and positive surface charge (+15 to +25 mV) (Fig. 2). Repetitive measurements in time show that the particles formed with HSA were stable for at least one month at room temperature.

Table 1 gives the loading efficiencies of the PAA/HSA nanoparticles at neutral pH, as determined by fluorescence spectroscopy measurements. It can be seen that the incorporation of the protein into the polymer nanoparticles is very high, even under the very dilute conditions applied (HSA concentration is 120 μg/ml). This demonstrates that the PAA polymers are capable to bind this protein with slightly net negative charge with high affinity. The fact that the p(CBA-ABOL) nanoparticles have a somewhat higher protein loading efficiency than the p(BAP-ABOL) nanoparticles may be due to the higher flexibility of the polymer backbone of the former polymer.

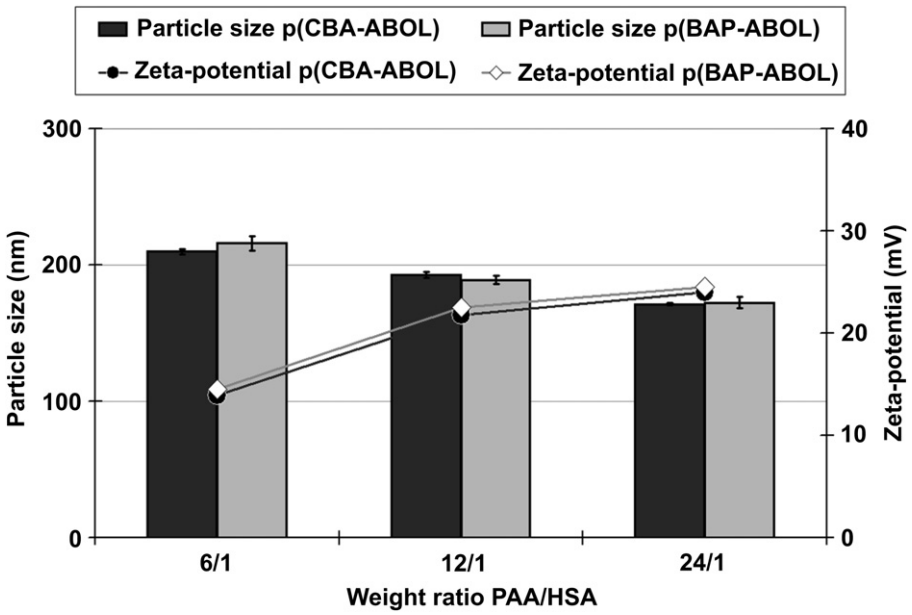

Fig. 2. Size distributions and zeta-potentials of nanoparticles of PAA/HSA in 10 mM HEPES buffer solution pH 7.4 measured by DLS at 25 °C at different PAA/HSA weight ratios, using p(CBA-ABOL) (black bars) and p(BAP-ABOL) (gray bars) as polymeric carrier.

3.4. Mimicking the intracellular disassembly of the p(CBA-ABOL)/protein nanoparticles in reducing environment

The rapid cleavage of the disulfide linkages in the p(CBA-ABOL) polymer in the intracellular environment due to the presence of glutathione and reductase enzymes can be favorably exploited to induce disassembly of the nanocomplexes resulting in efficient protein release. Table 2, column A, gives the percentages of HSA released from the p(CBA-ABOL) and p(BAP-ABOL) nanoparticles after incubation with 2.5 mM DTT for 30 min, as measured by fluorescence of the supernatant solution after centrifugation. The nanoparticles from the disulfide polymer p(CBA-ABOL) have released most of the encapsulated protein, due to the fast degradation of these polymers, whereas no release of protein was measured for the particles containing p(BAP-ABOL), the polymer lacking the disulfide linkages.

The results from these experiments suggest that once the p(CBA-ABOL) nanoparticles have arrived in the reductive environment inside the cell, HSA is released from the nanoparticles, due to the rapid cleavage of the disulfide linkages in the polymer backbone. In contrast, the release from nanoparticles made of p(BAP-ABOL) will be a much slower process, most probably mainly governed by destabilization of the nanoparticles upon acidification (*vide infra*) and/or the hydrolysis of the polymeric carrier. The distinct difference in protein release between the two polymeric carriers offers opportunities to tune the bioresponsive release by variation of the amount of disulfide linkages in the polymer chain of PAAs [25].

Table 1
HSA loading efficiencies of PAA/FITC-HSA nanoparticles prepared using different PAA/HSA weight ratios.

Polymer	Polymer/Protein weight ratio	FITC-HSA loading efficiency (%)[a]
p(CBA-ABOL)	6/1	89
	12/1	94
	24/1	97
p(BAP-ABOL)	6/1	73
	12/1	85
	24/1	90

[a] Percentage of HSA incorporated in the PAA nanoparticles (±1) in HEPES buffer solution.

3.5. Effect of environmental acidification on the nanoparticles

Since electrostatic interactions between the positively-charged polymer and the negatively-charged protein are an important, if not determining driving force for the self assembly into the nanoparticles, it can be expected that a decrease of the pH, as occurring during endosomal acidification, will also influence the stability of the nanoparticles. On one hand, a decrease of the pH will lead to a decrease of the amount of negative charges on the protein. On the other hand, the degree of protonation of the PAAs will be increased. Therefore there is a delicate balance between these effects, in which it is, however, expected that the decrease of overall negative charge on the protein will be the dominating factor, since an excess of positive charge is already present on the polymers in the nanoparticles at pH 7.4. Then, a decrease of the pH will lead to destabilization of the nanocomplexes and eventually release of the protein. DLS measurements show that the PAA/HSA nanoparticles significantly increase in size from *ca.* 165 nm to more than 300 nm when the pH decreases from 7.4 (extracellular pH) to 5.1 (endosomal pH) (Fig. 3). For both systems, small peaks in size distribution were observed around 40–50 nm when the pH is decreased to values below pH 5.3, revealing the formation of small aggregates of free protein.

The amount of released protein from the PAA/HSA nanoparticles after incubating the nanoparticle solution for 30 min at pH 5.1, and

Table 2
The extent of HSA release from p(BAP-ABOL)/FITC-HSA nanoparticles in HEPES buffer pH 7.4 (weight ratio 24/1), after addition: DTT to a final concentration of 2.5 mM (column A) or 0.25 M HCl to decrease pH down to pH 5.1 (column B).

Polymer	A (2.5 mM DTT)[a]	B (pH 5.1)[a]
p(CBA-ABOL)	93.9	14.0
p(BAP-ABOL)	1.8	17.0

[a] Percentage of HSA that is released from the polymeric nanoparticles (±1). Initial HSA concentration in the nanoparticles is 120 μg/ml.

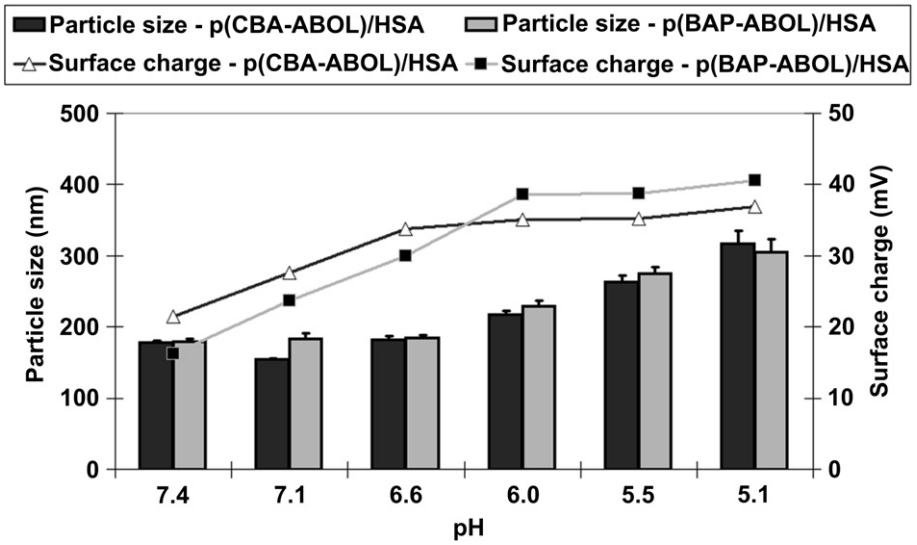

Fig. 3. Size distributions of nanoparticles of p(BAP-ABOL)/HSA (weight ratio 24:1) during pH titration of the particle solution from pH 7.4 to pH 5.1 (titration duration: 2 h), representing the pH of the extracellular and intracellular environments respectively, using p(CBA-ABOL) (black bars), and p(BAP-ABOL) (gray bars) as polymeric vector.

subsequent centrifugation of the nanoparticles is given in Table 2, column B. The HSA release is in the range of 14–17%, and obviously there is no clear difference between the two polymers whether it contains disulfide bonds or not. These results suggest that endosomal acidification alone may not be sufficient to release the protein content from the nanocomplexes and that bioreduction of the polymer backbone can give an essential contribution to the intracellular release process.

3.6. Cytotoxicity

A primary step in evaluating uptake of nanoparticles by the intestinal cells was to validate cell viability under the experimental conditions of uptake. The viability of Caco-2/TC7 cells after 48 h of incubation with the free p(CBA-ABOL) and p(BAP-ABOL) polymers, free HSA protein, as well as the polymer/HSA nanocomplexes was evaluated by BCA and alamar blue assays. Fig. 4 shows that the free HSA (12 mg/ml) and free p(CBA-ABOL) (288 mg/ml) were found to be non-cytotoxic, but the same concentration of p(BAP-ABOL) polymer induced a decrease in the total protein of *ca.* 15% after 48 h of exposure, reflecting decrease in the viable cell number adhering to the substratum. A similar level of cell viability was confirmed by the alamar blue assay that showed ~20% decrease of cell viability after 4 h of exposure to p(BAP-ABOL) and ~45% after 24–48 h of exposure. The p(CBA-ABOL)/HSA and p(BAP-ABOL)/HSA nanoparticles in the same concentrations as their uncomplexed free components exhibited similar toxicity. The Caco-2/TC7 cells were also exposed to nanoparticles in the presence of the non-specific multi drug resistance (MDR) blocker, CsA, in order to determine the possible involvement of the MDR machinery in the efflux of PAA/protein nanoparticles (*vide infra*). The presence of CsA appeared to be not cytotoxic after 4 h of incubation, but a slightly decreased cell viability of *ca.* 15% was found 24–48 h of exposure.

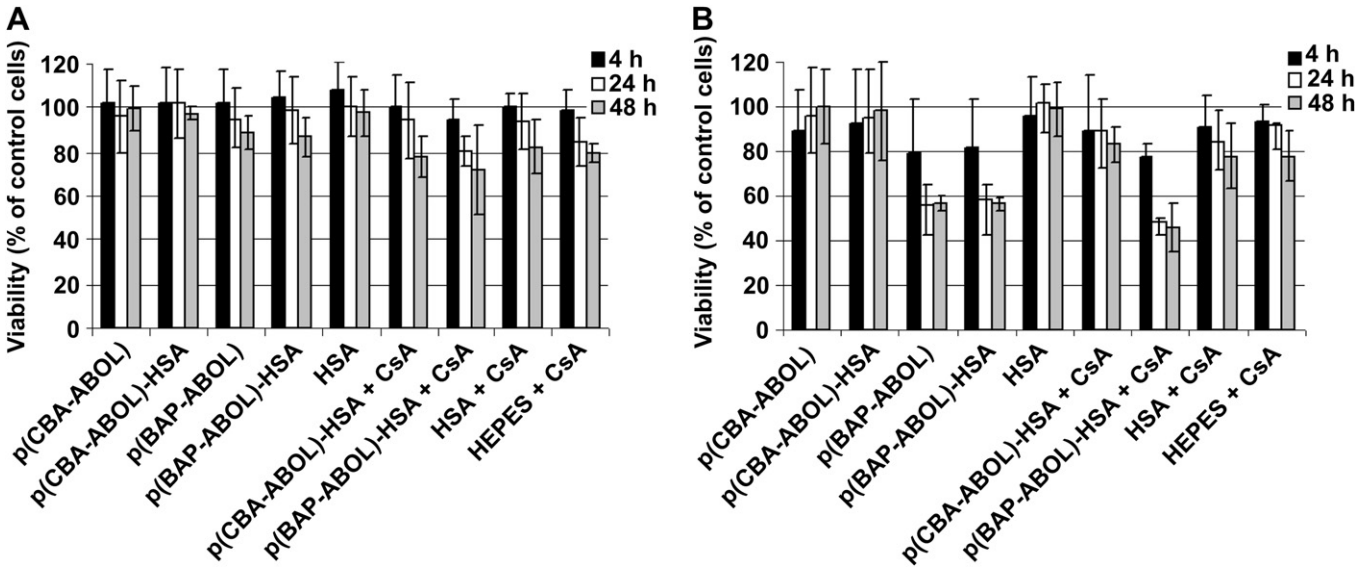

Fig. 4. Cell viability of Caco-2/TC7 cells following incubation with p(CBA-ABOL)/HSA and p(BAP-ABOL)/HSA nanoparticles, free polymers and HSA, in the presence and absence of CsA for 4 h (black columns), 24 h (white columns) and 48 h (gray columns). Cell viability was determined by (A) BCA and (B) Alamar assays. Assays were carried out at 37 °C in 10% serum supplemented media in presence or absence of 10 μM CsA. Results are given as mean ± SD of three independent experiments.

3.7. Uptake of the PAA nanoparticles as determined by flow cytometry

The uptake of nanoparticles carrying proteins and the release of their cargo into the cytosol can serve as means of enabling protein-based therapeutic agents to interact with their intracellular targets. The facilitation of PAA nanoparticles to introduce HSA into the cytosol of Caco-2/TC7 cells was studied by FACS analysis of the cells exposed to the two types of PAA/HSA nanoparticles for 4 and 24 h. To verify that the fluorescence as measured in the FACS analysis originated from increased uptake of FITC-HSA in the cells, and not caused by residual nanoparticles adsorbed to the cell membrane, we have analyzed by FACS the fluorescence intensity of cells exposed at 4 °C to HSA, p(CBA-ABOL) and p(BAP-ABOL), either in complex or alone. At 4 °C the endocytic machinery is not active [36], thereby enabling only adsorption of nanoparticles to the cell membrane. The signals detected in these cells, under this condition of low temperature, were found to be very low and comparable to the auto-fluorescence of non-treated cells. Fig. 5 shows the relative fluorescent intensities obtained from Caco-2/TC7 cells exposed to free HSA and to the two polymer/HSA nanoparticles after 4 and 24 h of exposure, in the absence and presence of CsA. Low fluorescence intensities were detected when cells were incubated with solutions of free HSA, indicating a poor uptake of the free protein, which is in line with previous studies [37,38]. However, a significant increase of fluorescence intensity for HSA uptake was obtained when cells were incubated with p(CBA-ABOL)/HSA nanoparticles. After 4 h, these cells exhibited *ca.* 1.5 fold ($p < 0.05$) higher fluorescence level than cells exposed to free HSA, and after 24 h of exposure this level increased to *ca.* 4 fold ($p < 0.01$). In comparison, the uptake of HSA carried by p(BAP-ABOL)/FITC-HSA nanoparticles was similar to that of free HSA, indicating no improvement of uptake and almost no uptake of these particles. These results demonstrate that the nanoparticles made of the p(CBA-ABOL) polymer have superior capacity to deliver HSA into the cells, than those possessed by the polymer lacking disulfide bonds of p(BAP-ABOL).

As uptake of nanoparticles is the net outcome of two competing influx and efflux processes of the particles, we employed CsA as non-specific inhibitor for the efflux pumps associated with the MDR family. Fig. 5 shows that exposure of Caco-2/TC7 cells to p(CBA-ABOL)/HSA nanoparticles in the presence of 10 μM CsA yielded a significant increase of HSA uptake of ~2.8 folds ($p < 0.001$) and ~5 folds ($p < 0.001$), after 4 and 24 h of exposure, respectively. In contrast, the FITC emission intensities of cells exposed to p(BAP-ABOL)/HSA nanoparticles were not affected by the presence of CsA. These findings demonstrate that p(CBA-ABOL)/HSA nanoparticles undergo an efficient influx as well as extrusion via CsA sensitive efflux pumps. The observed low protein delivery by p(BAP-ABOL) nanoparticles may be attributed either to a very low influx or to an efficient removal of the p(BAP-ABOL)/HSA nanoparticles from the cells through efflux pathways which are insensitive to CsA.

3.8. Effect of mucus level on the uptake of PAA/protein nanoparticles

As mucus covers the cell layer of intestinal epithelium, composed of enterocytes and mucus secreting goblet cells, we have chosen to examine uptake in co-cultures of Caco-2/TC7 and HT29-MTX mucus secreting cells. Different ratios of Caco-2/TC7 and HT29-MTX were mixed and the extent of uptake of p(CBA-ABOL)/HSA nanoparticles as well as p(BAP-ABOL)/HSA nanoparticles was determined by flow cytometry analysis, following 4 and 24 h of exposure (Fig. 6A and B, respectively). It was shown that the uptake of free HSA was not altered with increase of the percentage of HT29-MTX cells in the cell culture. However, the uptake of the HSA-loaded p(CBA-ABOL) nanoparticles increased significantly in a linear fashion upon increment of the percentage of HT29-MTX cells in the cell co-cultures, both after 4 h and 24 h of exposure. When a homogeneous population of HT29-MTX cells, (corresponding to Caco-2/TC7:HT29-MTX ratio of 0:100) was exposed to these nanoparticles, FITC emission intensity of HSA was 5 folds

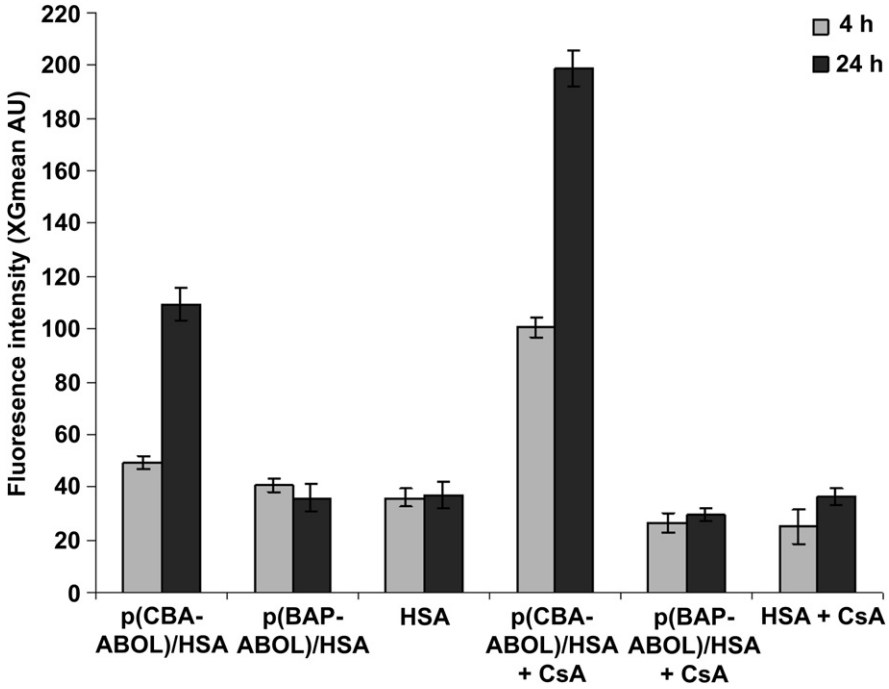

Fig. 5. Uptake of PAA/HSA nanoparticles by Caco-2/TC7 cells as measured by flow cytometry. Exposure to p(CBA-ABOL)/HSA, p(BAP-ABOL)/HSA and free HSA was carried out for 4 (gray columns) and 24 (black columns) hours at 37 °C, in the absence or presence of 10 μM CsA. The uptake is given as in terms of the geometrical mean (XGmean) ± SD of fluorescence distribution of 10,000 cells in three independent experiments ($n = 3$).

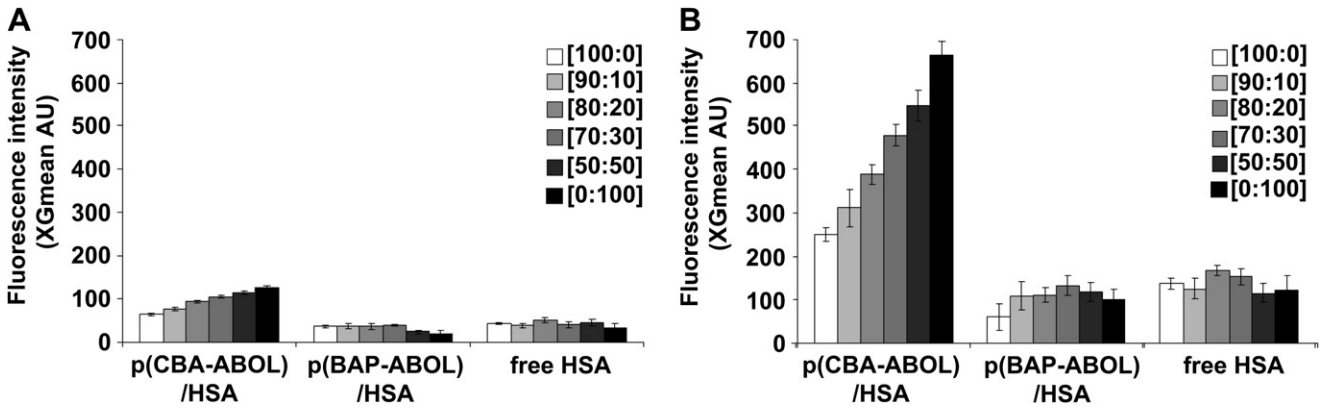

Fig. 6. Uptake of PAA/HSA nanoparticles by different ratios of Caco-2/TC7:HT29-MTX co-cultures exposed to p(CBA-ABOL)/HSA, p(BAP-ABOL)/HSA nanoparticles and free HSA for 4 h (A) and 24 h (B) at 37 °C. The uptake is given as in terms of the geometrical mean (XGmean) ± SD of fluorescence distribution of 10,000 cells in three independent experiments ($n = 3$).

higher than those of cells exposed to free HSA. In contrast, the uptake of the p(BAP-ABOL)/HSA nanoparticles was not affected by an increase of HT29-MTX percentage in the cell co-culture and remained constant even after 24 h of exposure, with extent of uptake similar or even lower than for the uptake of free HSA, illustrating a poor intracellular delivery capacity. It may be suggested that both the presence of mucus produced by the HT29-MTX cells as well as the presence of the disulfide bonds of p(CBA-ABOL) are involved in the enhanced uptake of these nanoparticles. These results are in good agreement with the rheological experiments showing that the p(CBA-ABOL) polymer interacts strongly with mucus, in contrast to p(BAP-ABOL) lacking disulfide linkages.

3.9. Compartmental localization of polymer/protein nanoparticles by confocal microscopy

The uptake of the PAA/HSA nanoparticles and their subsequent localization in Caco-2/TC7 cells were examined by confocal microscopy. Cells were incubated with free HSA, p(CBA-ABOL)/HSA and p(BAP-ABOL)/HSA nanoparticles, as well as free p(CBA-ABOL) and p(BAP-ABOL) polymers. The confocal microscopy images of Caco-2/TC7 cells exposed to free FITC-HSA (Fig. 7B) showed no significant fluorescence signal, similar to the non-treated cells (Fig. 7A), indicating that free HSA was not taken up by these cells. The free polymers were used as control and indeed,

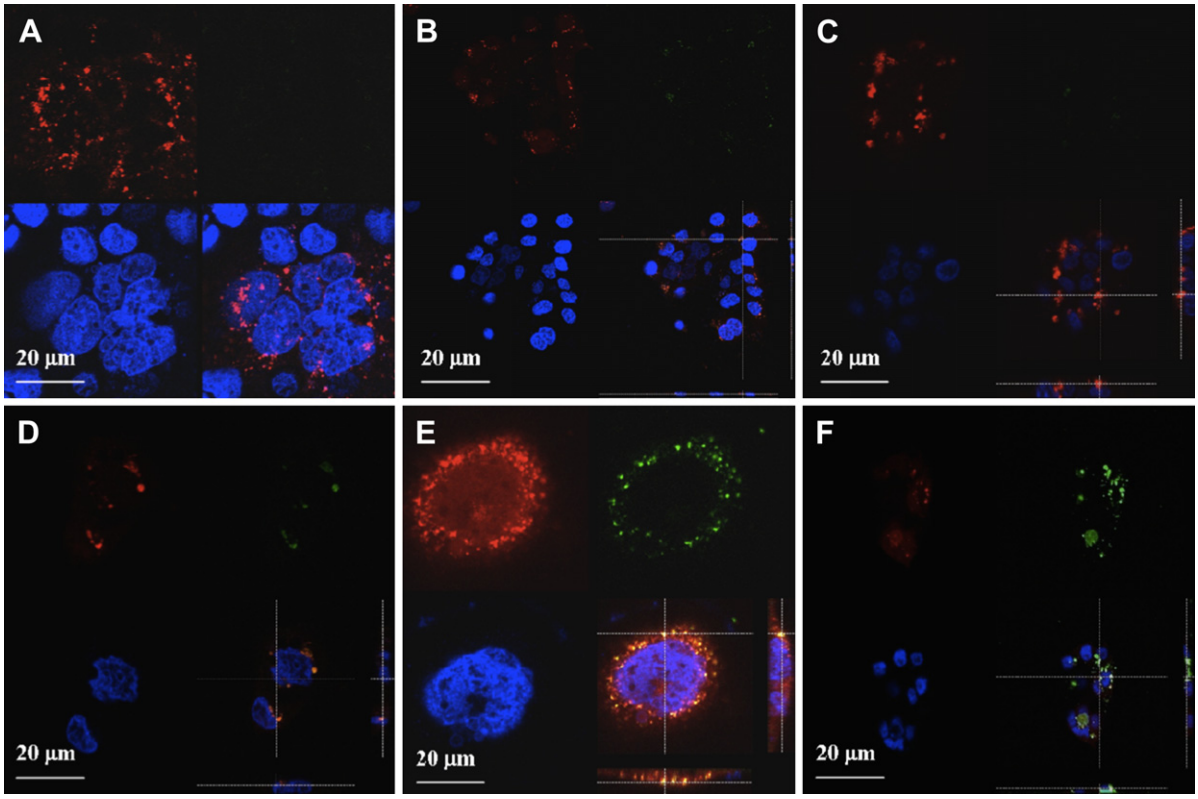

Fig. 7. Median optical sections of confocal z-stack of Caco-2/TC7 cells exposed to nanoparticles for 24 h at 37 °C. A: non-treated cells, B: free HSA, C: free p(CBA-ABOL), D: free p(BAP-ABOL), E: p(CBA-ABOL)/HSA nanoparticles, F: p(BAP-ABOL)/HSA nanoparticles. Red: LysoTracker probe; Blue: Hoechst nuclear staining; Green: FITC labeled – HSA. Each panel is composed of 3 channels: green, red, blue and a merged image. In the right and bottom part of the panels B–F are placed orthogonal cross sections of the Z-stack. (For interpretation of the references to color in this figure legend, the reader is referred to the web version of this article.)

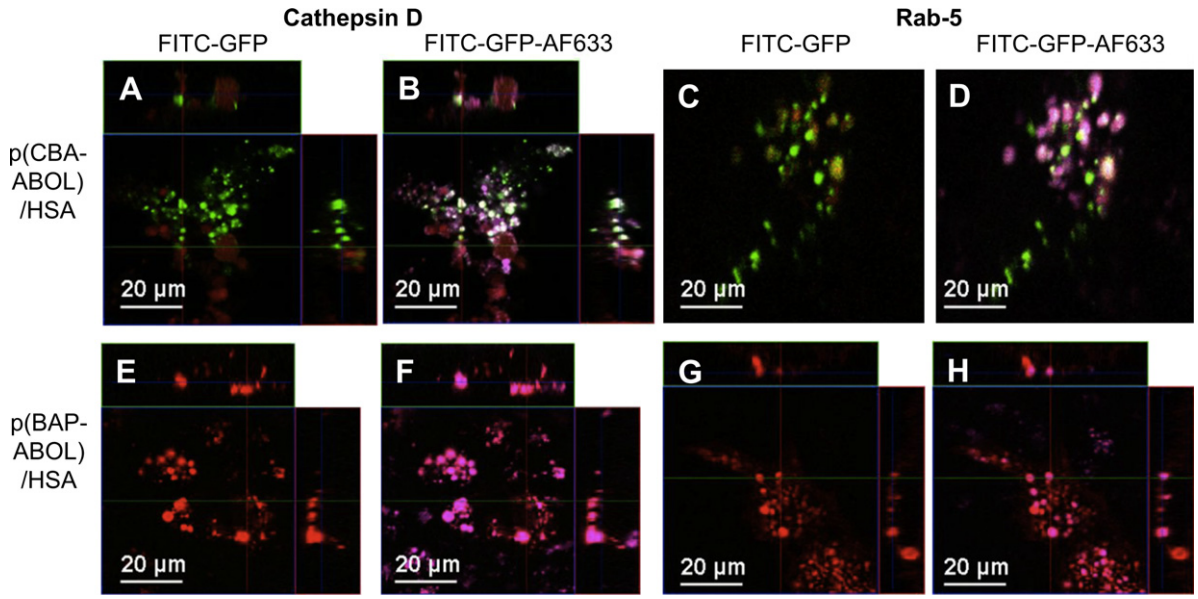

Fig. 8. Median optical sections of confocal z-stack of Caco-2/TC7 cells expressing Cathepsin-D-RFP (A, B; E, F) or Rab-5-RFP (C, D; G, H) exposed to p(CBA-ABOL)/HSA (A, B; C, D) or p(BAP-ABOL)/HSA (E, F; G, H) nanoparticles for 24 h. Green: FITC-HSA, Red: Red fluorescence protein (RFP), Pink: AF633-labeled polymers, White: colocalization of red, green and pink fluorophores. In the right and bottom part of the panels A–B, E–H are placed orthogonal cross sections of the Z-stack. (For interpretation of the references to color in this figure legend, the reader is referred to the web version of this article.)

as expected, very low green signal was observed when cells were exposed to the free polymers (Fig. 7C and D); the low fluorescence signal which is still apparent may originate from the green autofluorescence of the Caco-2/TC7 cells. The p(CBA-ABOL)/HSA nanocomplexes clearly demonstrated to be internalized into cells as they are seen as green-red co-localized aggregates, within the cell cytosol and lysosomal compartments following 24 h of exposure (Fig. 7E). In contrast, the low level of FITC signal in cells exposed to p(BAP-ABOL)/HSA nanoparticles was similar to that found in cells exposed to the same amount of free FITC-HSA. Most of the weak FITC fluorescence level that was observed in these cells seemed to be adsorbed on the cell membrane and not within the cytoplasm, suggesting that these nanoparticles were poorly internalized (Fig. 7F).

In order to localize the nanoparticles in the different endosomal compartments, Caco-2/TC7 cells expressing either Rab-5 (early endosomes) or Cathepsin D (lysosomes) tagged with red fluorescent protein were incubated with the HSA-loaded nanoparticles. Cells incubated with p(CBA-ABOL)/HSA nanoparticles showed green FITC-HSA dots in the cytosol, and white aggregates. The later representing the colocalization of the red fluorescence protein from the endosomal or lysosomal compartments, with the AF633-labeled polymer (pink) and FITC-HSA (green) (Fig. 8A–D). As not all the green dots that were observed were localized within the analyzed compartments, it may suggest that HSA dissociated from the p(CBA-ABOL)/HSA nanocomplex and was released into the cytosol. In contrast, cells exposed to p(BAP-ABOL)/HSA nanoparticles did not contain any co-localized green-red markers, but possessed only weak green dots in the cytoplasm that were not co-localized with endosomal markers, indicating that HSA was poorly internalized (Fig. 8E–H). These results clearly confirm the higher capacity of the p(CBA-ABOL) polymer as carrier for intracellular delivery of HSA, in comparison to the p(BAP-ABOL) polymer, lacking disulfide bonds. In addition, when the cells were exposed to HSA-loaded nanoparticles made of Rhodamine B labeled CBA-ABOL, their cytoplasm exhibits a much broader spread of red than cells exposed to HSA-loaded nanoparticles made of p(BAP-ABOL) (data not shown). This distributed red pattern is most likely due to the reduction of the disulfide bonds within p(CBA-ABOL) in the cell as a result of the reductive environment prevailing in the cytosol, involving degradation of the polymer. This observation is in good agreement with the results given in Table 2A depicting higher intracellular protein release from the nanoparticles made of the p(CBA-ABOL) polymers in the presence of the reducing agent DTT.

4. Conclusions

Both positively-charged PAAs, p(CBA-ABOL) and p(BAP-ABOL), can self-assemble with the net negatively-charged protein HSA to form stable nanosized complexes at physiological pH 7.4. Acidification to pH 5.1 leads to destabilization of the nanocomplexes, which may serve as an indication that such a process also occurs after endosomal uptake. Since p(CBA-ABOL) induces much higher viscosity to intestinal mucus than p(BAP-ABOL) it might be expected that protein-loaded nanoparticles with disulfide moieties give higher mucoadhesion in the intestine. This is also supported by the high correlation between the extent of uptake of p(CBA-ABOL)-based nanoparticles and the mucus level of the cell culture, a phenomenon that was not detected for p(BAP-ABOL), lacking the disulfide bonds. In addition, p(CBA-ABOL) nanoparticles show fast disintegration in reductive solution, indicating that the protein payload will become quickly released in the intracellular environment. Indeed, HSA, complexed with p(CBA-ABOL) into nanoparticles was successfully internalized into Caco-2/TC7 cells and after cellular uptake, the protein-containing p(CBA-ABOL) nanocomplexes became disassembled and HSA was released inside the cell with excellent cell viability. The internalization efficiency using p(CBA-ABOL) nanoparticles was further enhanced in the presence of CsA, suggesting that a counteracting MDR-dependent efflux pathway is mitigating the efficacy of these nanoparticles. In contrast to the HSA-p(CBA-ABOL) nanoparticles, the HSA-p(BAP-ABOL) nanoparticles show only low intracellular protein delivery. The fluorescence cytometry and confocal microscopy results for HSA-p(BAP-ABOL) nanoparticles suggest adsorption of these nanoparticles to the cell membrane rather than intracellular uptake.

Acknowledgments

This research work is part of the Integrated European FP6 IP NanoBioPharmaceutics (# 026723-2).

References

[1] Owens DR, Zinman B, Bolli G. Alternative routes of insulin delivery. Diabetic Med 2003;20:886–98.
[2] Merkle HP. New aspects of pharmaceutical dosage forms for controlled drug-delivery of peptides and proteins. Eur J Pharm Sci 1994;2:19–21.
[3] Manning MC, Patel K, Borchardt RT. Stability of protein pharmaceuticals. Pharm Res 1989;6:903–18.
[4] Tabata Y, Ikada Y. Protein release from gelatin matrices. Adv Drug Deliv Rev 1998;31:287–301.
[5] Lehr CM. Bioadhesion technologies for the delivery of peptide and protein drugs to the gastrointestinal tract. Crit Rev Ther Drug Carr Syst 1994;11:119–60.
[6] Couvreur P, Puisieux F. Nanoparticles and microparticles for the delivery of polypeptides and proteins. Adv Drug Deliv Rev 1993;10:141–62.
[7] Kreuter J. Peroral administration of nanoparticles. Adv Drug Deliv Rev 1991;7:71–86.
[8] Bernkop-Schnürch A. Thiomers: a new generation of mucoadhesive polymers. Adv Drug Deliv Rev 2005;57:1569–82.
[9] Dufresne MH, Gauthier MA, Leroux JC. Thiol-functionalized polymeric micelles: from molecular recognition to improved mucoadhesion. Bioconjug Chem 2005;16:1027–33.
[10] Bernkop-Schnürch A, Schwarz V, Steininger S. Polymers with thiol groups: a new generation of mucoadhesive polymers? Pharm Res 1999;16:876–81.
[11] Kafedjiiski K, Foger F, Bernkop-Schnürch A, Werle M. Evaluation of *in vitro* enzymatic degradation of various thiomers and cross-linked thiomers. Drug Dev Ind Pharm 2007;33:199–208.
[12] Marschutz MK, Caliceti P, Bernkop-Schnürch A. Design and *in vivo* evaluation of an oral delivery system for insulin. Pharm Res 2000;17:1468–74.
[13] Boussif O, Lezoualch F, Zanta MA, Mergny MD, Scherman D, Demeneix B, et al. A versatile vector for gene and oligonucleotide transfer into cells in culture and in-vivo – polyethylenimine. Proc Natl Acad Sci U S A 1995;92:7297–301.
[14] Eichman JD, Bielinska AU, Kukowska-Latallo JF, Baker Jr JR. The use of PAMAM dendrimers in the efficient transfer of genetic material into cells. Pharmaceut Sci Tech Today 2000;3:232–45.
[15] Ranucci E, Spagnoli G, Ferruti P, Sgouras D, Duncan R. Poly(amidoamine)s with potential as drug carriers: degradation and cellular toxicity. J Biomater Sci Polym Ed 1991;2:303–15.
[16] Wu GY, Wu CH. Receptor-mediated in vitro gene transformation by a soluble DNA carrier system. J Biol Chem 1987;262:4429–32.
[17] Franchini J, Ranucci E, Ferruti P. Synthesis, physicochemical properties, and preliminary biological characterizations of a novel amphoteric agmatine-based poly(amidoamine) with RGD-like repeating units. Biomacromolecules 2006;7:1215–22.
[18] Ferruti P, Marchisio MA, Duncan R. Poly(amido-amine)s: biomedical applications. Macromol Rapid Commun 2002;23:332–55.
[19] Lavignac N, Lazenby M, Franchini J, Ferruti P, Duncan R. Synthesis and preliminary evaluation of poly(amidoamine)-melittin conjugates as endosomolytic polymers and/or potential anticancer therapeutics. Int J Pharm 2005;300:102–12.
[20] Lavignac N, Nicholls JL, Ferruti P, Duncan R. Poly(amidoamine) conjugates containing doxorubicin bound via an acid-sensitive linker. Macromol Biosci 2009;9:480–7.
[21] Pattrick NG, Richardson SCW, Casolaro M, Ferruti P, Duncan R. Poly(amidoamine)-mediated intracytoplasmic delivery of ricin A-chain and gelonin. J Control Release 2001;77:225–32.
[22] Swaminathan S, Cavalli R, Trotta F, Ferruti P, Ranucci E, Gerges I, et al. *In vitro* release modulation and conformational stabilization of a model protein using swellable polyamidoamine nanosponges of beta-cyclodextrin. J Incl Phenom Macrocycl Chem 2010;68:183–91.
[23] Coué G, Engbersen JFJ. Functionalized linear poly(amidoamine)s are efficient vectors for intracellular protein delivery. J Control Release 2011;152:90–8.
[24] Piest M, Lin C, Mateos-Timoneda MA, Lok MC, Hennink WE, Feijen J, et al. Novel poly(amido amine)s with bioreducible disulfide linkages in their diamino-units: structure effects and in vitro gene transfer properties. J Control Release 2008;130:38–45.
[25] Lin C, Zhong Z, Lok MC, Jiang X, Hennink WE, Feijen J, et al. Linear poly(amido amine)s with secondary and tertiary amino groups and variable amounts of disulfide linkages: synthesis and *in vitro* gene transfer properties. J Control Release 2006;116:130–7.
[26] Lin C, Zhong Z, Lok MC, Jiang X, Hennink WE, Feijen J, et al. Random and block copolymers of bioreducible poly(amido amine)s with high- and low-basicity amino groups: study of DNA condensation and buffer capacity on gene transfection. J Control Release 2007;123:67–75.
[27] Lin C, Zhong Z, Lok MC, Jiang X, Hennink WE, Feijen J, et al. Novel bioreducible poly(amido amine)s for highly efficient gene delivery. Bioconjug Chem 2007;18:138–45.
[28] Mateos-Timoneda MA, Lok MC, Hennink WE, Feijen J, Engbersen JFJ. Poly-(amido amine)s as gene delivery vectors: effects of quaternary nicotinamide moieties in the side chains. ChemMedChem 2008;3:478–86.
[29] Akinc A, Thomas M, Klibanov AM, Langer R. Exploring polyethyleniminemediated DNA transfection and the proton sponge hypothesis. J Gene Med 2005;7:657–63.
[30] Yang S, May S. Release of cationic polymer-DNA complexes from the endosome: a theoretical investigation of the proton sponge hypothesis. J Chem Phys 2008;129:185105.
[31] Watson P, Jones AT, Stephens DJ. Intracellular trafficking pathways and drug delivery: fluorescence imaging of living and fixed cells. Adv Drug Deliv Rev 2005;57:43–61.
[32] Lin C, Engbersen JFJ. The role of the disulfide group in disulfide-based polymeric gene carriers. Expert Opin Drug Deliv 2009;6:421–39.
[33] Rajender KC, Frederick WL, Michael HK, David MB, Robert GBR, Daniel R. Plasma cysteine, cystine, and glutathione in cirrhosis. Gastroenterology 1984;87:770–6.
[34] Lin C, Engbersen JFJ. Effect of chemical functionalities in poly(amido amine)s for non-viral gene transfection. J Control Release 2008;132:267–72.
[35] Calvo P, RemunanLopez C, VilaJato JL, Alonso MJ. Novel hydrophilic chitosan-polyethylene oxide nanoparticles as protein carriers. J Appl Polym Sci 1997;63:125–32.
[36] Desai MP, Labhasetwar V, Walter E, Levy RJ, Amidon GL. The mechanism of uptake of biodegradable microparticles in caco-2 cells is size dependent. Pharm Res 1997;14:1568–73.
[37] Gu SC, Papadopoulou N, Gehring EM, Nasir O, Dimas K, Bhavsar SK, et al. Functional membrane androgen receptors in colon tumors trigger pro-apoptotic responses *in vitro* and reduce drastically tumor incidence *in vivo*. Mol Cancer 2009;8:114.
[38] Wasan EK, Waterhouse D, Sivak O, Bally MB, Klasa RJ, Wasan KM. Plasma protein binding, lipoprotein distribution and uptake of free and lipid-associated BCL-2 antisense oligodeoxynucleotides (G3139) in human melanoma cells. Int J Pharm 2002;241:57–64.